www.czasopisma.pan.pl PAN POLSKA AKADEMIA NAUK www.journals.pan.pl

Arch. Metall. Mater. **67** (2022), 2, 421-433

DOI: https://doi.org/10.24425/amm.2022.137773

ZEHUA LV[1,2,3], ZHIXIONG ZHANG[1,2,3], JIANCHAO HAN[1,2,3], TAO WANG[1,2,3*]

# INFLUENCE OF ANNEALING TREATMENT ON DEEP DRAWING BEHAVIOR OF Q235 CARBON STEEL /410/304 STAINLESS STEELS THREE-LAYER COMPOSITE PLATE

Effect of annealing treatment on deep drawing behavior of hot-rolled Q235 carbon steel/410/304 stainless steel three-layer composite plate was investigated. Deep drawability of the unannealed composite plates exhibits a sharp difference for various contact surfaces with the die. The limit drawing ratio (LDR) of the composite plate with the carbon steel contacting the die is 1.75, while it is 1.83 with the stainless steel contacting the die due to the different mechanical responses to the tensile stress at the corner of the die. After annealing at 900°C for 2 h, however, the deep drawabilities of the composite plates both for various contact surfaces with the die are significantly improved and becomes almost identical, which are attributed to the stress relief, the enhanced ductility and the improved interface bonding strength of the hot-rolled component plates during annealing.

*Keywords:* composite plate; deep drawing; annealing; microstructure

## 1. Introduction

Carbon steel-stainless steel composite plates can provide both the excellent corrosion resistance of stainless steel and the high mechanical properties and low cost of carbon steel [1], which are widely used in the petroleum and chemical industries and water conservancy facilities and so on [2]. Several processing techniques, such as explosive welding, diffusion bonding, vacuum brazing, transient-liquid-phase bonding, hot pressing, casting, and roll bonding, were used to fabricate stainless steel clad plates [3-4]. Among them, hot roll bonding is the most economic and productive manufacturing process for large bi-layered metal clad plates and multilayered metal clad plates [5]. Microstructure evolution and mechanical properties of carbon steel-stainless steel bilayer composite plates fabricated by hot rolling method have been well investigated [6-11].

Formability is an important evaluation criterion of metal sheets [12-14]. Deep drawing is one of the frequently-used stamping methods [15-16], which is often measured by limit drawing ratio (LDR), namely, the maximum blank diameter/punch diameter without the appearance of cracks and wrinkles during deep drawing. However, deep drawing of stainless steel composite plate was hardly reported. There were only some reports about individual carbon steel or stainless steel plate. Tokar et al. [17] gave failure analysis at deep drawing of low carbon steels, indicated the interface cementite particle/ferrite matrix is the main reason for microcrack formation and the reduction in deep drawing capacity of steel. Padmanabhan et al. [18] investigated the effects of die radius, blank holder force and friction coefficient on the deep-drawing of a stainless steel axi-symmetric cup through finite element method, indicating that die radius had the greatest influence on the deep drawing followed by the blank holder force and the friction coefficient. Lade et al. [19] observed the microstructure variations of SUS 304 stainless steel at LDR when the cup was drawn at various temperatures wherein the highest LDR was obtained at 150°C in the absence of strain-induced martensite.

Martensitic 410 stainless steel has good corrosion resistance and excellent machinability, and also much cheaper than austenitic 304 stainless steel. For the consideration of plate quality and cost, thinning the 304 stainless steel and replacing part of it with 410 stainless steel in the clad plate can further save the cost without affecting the performance of the clad plate. In this paper, a cheaper Q235/410/304 stainless steels three-layer composite plate with high performance was fabricated by hot rolling, wherein Q235 carbon steel was used as base plate,

[1] TAIYUAN UNIVERSITY OF TECHNOLOGY, COLLEGE OF MECHANICAL AND VEHICLE ENGINEERING, TAIYUAN 030024, PR CHINA
[2] TAIYUAN UNIVERSITY OF TECHNOLOGY, ENGINEERING RESEARCH CENTER OF ADVANCED METAL COMPOSITES FORMING TECHNOLOGY AND EQUIPMENT, MINISTRY OF EDUCATION, TAIYUAN 030024, PR CHINA
[3] TAIYUAN UNIVERSITY OF TECHNOLOGY, TYUT-UOW JOINT RESEARCH CENTRE, TAIYUAN 030024, PR CHINA

* Corresponding author: tyut_wt@163.com

410 martensitic stainless steel as the interlayer and 304 austenitic stainless steel as the cladding plate. Liu et al. [6] reported that for C and Cr elements, the concentration gradient and diffusion coefficient were the main factors affecting the diffusion distance. This stacking method can reduce the concentration gradient of elements between plates, thin the over-thick decarburized layer (resulting in the decrease of fatigue resistance) and carburized layer (resulting in intergranular corrosion and the decrease of mechanical strength) caused by excessive difference in chemical potential, and obtain a stainless steel composite plate with better performance. The influences of contact faces of the three-layer composite plates with the punch and annealing treatment on the cold deep drawability of Q235 carbon steel/410/304 stainless steel composite plate was investigated. The reasons were analyzed by microstructure and interface structure, hardness and tensile mechanical behavior characterization.

## 2. Experimental procedure

### 2.1. Materials and cladding method

Q235B carbon steel as base plate with a dimension of 1100 mm×550 mm×23 mm was cut along the rolling direction. 304 stainless steel as cladding plate and 410 stainless steel as the interlayer had the same dimension of 1000 mm×500 mm×2.5 mm and were cut along the rolling direction. The chemical compositions of the three plates are shown in TABLE 1. The composite plate was hot-rolled symmetrically, and the stacking order from top to bottom was Q235, 410, 304, 304, 410, Q235 as shown in Figure 1. The two layers of the 304 stainless steel were isolated with isolation agent to ensure that the two composite plates could be separated after rolling. The billet was welded by submerged arc welding and vacuumed up to 1000 Pa. Then the welded billet was heated to 1030°C for 1 hour for 2-pass continuous rolling. The roll-bonding thickness reduction ratios of the first and second passes were 69% and 65%, respectively. The composite plates were rolled to 2.9 mm from an initial thickness of 28 mm. The individual thicknesses of Q235 carbon steel, 410 stainless steel and 304 stainless steel after rolling are about 2.4 mm, 0.25 mm, 0.25 mm, respectively. And the composite plate was air-cooled to room temperature after rolling. Finally, the bending deformation caused by rolling was removed by a straightening machine. A part of the rolled plates was annealed at 900°C for 2 hours and cooled in the furnace to room temperature.

### 2.2. Mechanical properties

#### 2.2.1. Hardness test

Vickers microhardness was measured with a HTV-1000 digit hardness tester across the matrices and the interfaces of the hot-rolled plates and annealed plates. A load of 200g and dwell time of 10s was applied.

TABLE 1

Chemical composition of raw materials (wt.%)

| Materials | C | Si | Mn | Cr | Ni | P | S | Cu | Mo | Co | N | Fe |
|---|---|---|---|---|---|---|---|---|---|---|---|---|
| Q235B | 0.206 | 0.187 | 0.792 | 0.021 | 0.017 | 0.018 | 0.01 | 0.021 | — | — | — | Bal. |
| 410 | 0.12 | 0.56 | 0.37 | 12.07 | — | 0.025 | 0.001 | — | — | — | — | Bal. |
| 304 | 0.036 | 0.43 | 0.94 | 18.15 | 8.03 | 0.03 | 0.006 | 0.019 | 0.004 | 0.233 | 0.043 | Bal. |

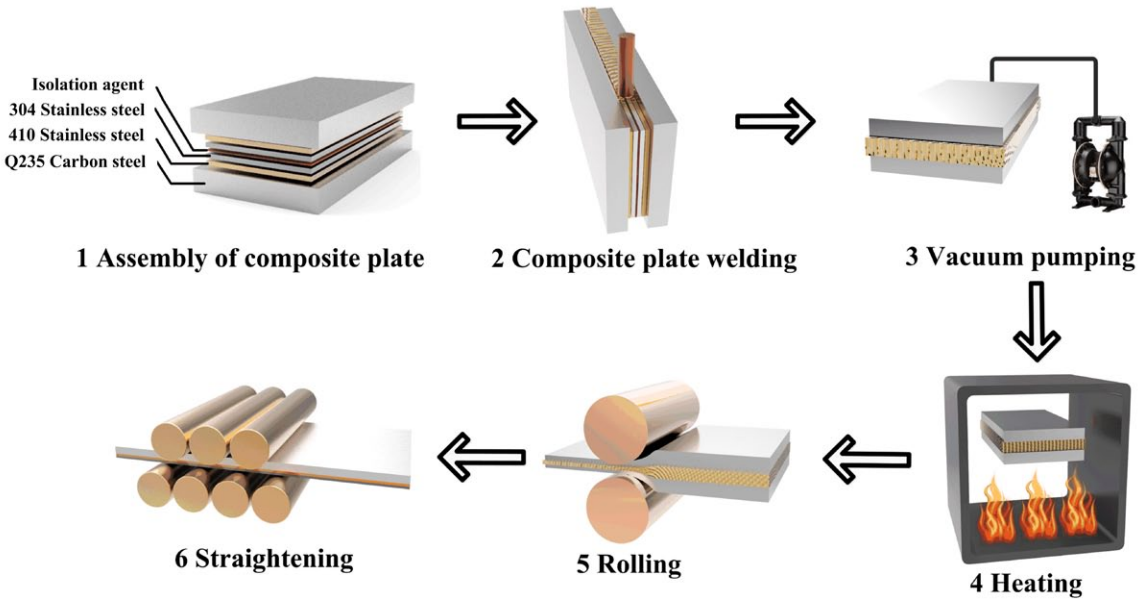


Fig. 1. Rolling flow diagram

### 2.2.2. Tensile test

Room-temperature tensile tests were conducted for the hot-rolled plates and annealed ones by Instron 5969 Universal Material Testing Machine according to ASTME8/E8M-2013a Standard Test Methods. Tensile specimens were cut along the rolling direction (RD), 45° direction and transverse direction (TD). The dog-bone shaped tensile specimens have the dimensions of the gauge length of 20 mm, the width of 5 mm and the thickness of 2.9 mm. The crosshead speed was 0.5 mm/min.

## 2.3. Deep drawing of Q235 carbon steel/410/304 stainless steel composite plate

Deep drawing was conducted on Genbon EC600 sheet metal forming test machine as shown in Figure 2(a) and 2(b). The fillets of the punch and the die were 10 mm and 5 mm, respectively. The diameters of punch and die were 60 mm and 66 mm, respectively. The samples are divided into four groups according to annealing or not and various contact surfaces. The hot-rolled composite plates are called group A with 304 stainless steel side in contact with the die and group B with carbon steel side contacting with the die. The annealed composite plates are termed as group C with 304 stainless steel side contacting with the die and group D with carbon steel side in contact with the die. The grouping is shown in TABLE 2.

Drawing tests were carried using circular blanks with various diameters to determine the LDR. The initial round blank diameter was set as 80 mm in the four groups. A similar deep drawing process was repeated in the next blank with the diameter increasing by 5 mm. The stainless steel surface and carbon steel surface of all samples were grinded with an angle grinder to remove the oxide layer and expose fresh metal, and the samples were quickly sent to the sheet forming machine for deep drawing. The blank holder force was dynamically adjusted by the negative feedback control system according to the metal flow, and the value fluctuates around 50 KN. Polytetrafluoroethylene (PTFE) and Vaseline were used to lubricate the upper surface of blank holder and punch, and the lower surface of die. The speed of the punch upward was 5mm/min. The thickness strain variations along three different directions (RD, 45°, TD) of the drawn cup were measured by using a micrometer every 2 mm to describe the uniformity of wall thickness distribution.

## 2.4. Characterization

Microstructure observation adjacent to the interfaces for the hot-rolled plate, annealed plate and deep-drawn cup were performed by optical microscope (OM) and scanning electron microscope (SEM) equipped with energy dispersive spectroscopy (EDS) to determine the interface microstructure variation and tensile fracture morphology. Roughness and three-dimensional (3D) topography of both surfaces of the hot-rolled plate and annealed plate were measured by shape measurement laser microscope. The solution of 50% $HNO_3$ + 50% $H_2O$ and 4g Picric

TABLE 2

Grouping of deep drawing experiments

| Group | The conditions of the annealing operation |
|---|---|
| Group A | The hot-rolled composite plates and 304 stainless steel contacts the die |
| Group B | The hot-rolled composite plates and Q235 carbon steel contacts the die |
| Group C | The annealed composite plates and 304 stainless steel contacts the die |
| Group D | The annealed composite plates and Q235 carbon steel contacts the die |

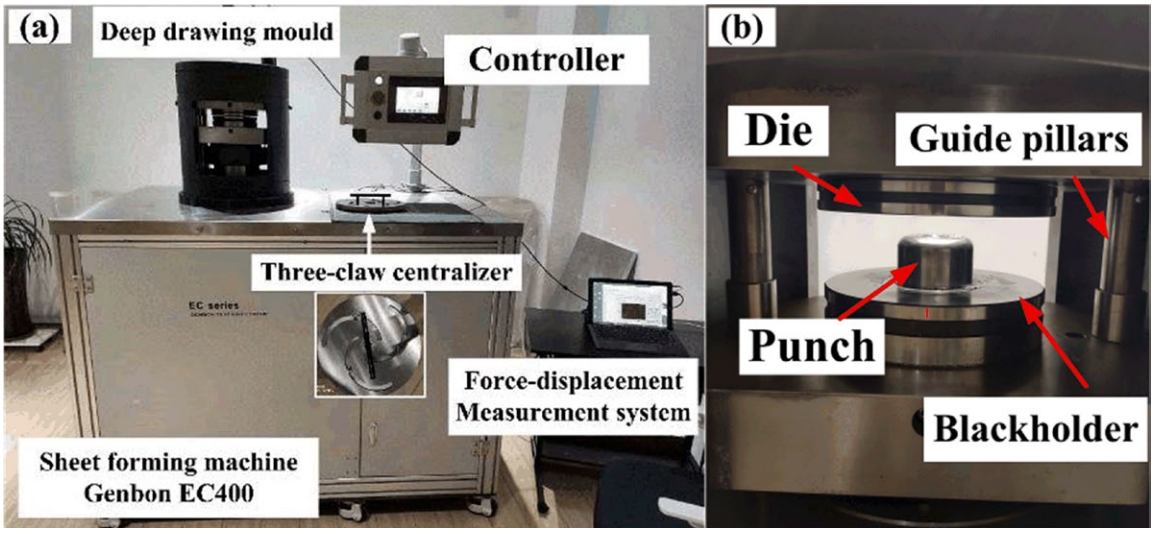


Fig. 2. (a) Deep drawing equipment and (b) forming mould

acid + 5ml HCl +100 ml $H_2O$ was used as the etchant to display the microstructure of 304 stainless steel and 410 stainless steel. 4% nitric acid in ethanol solution was used for carbon steel. A quarter of the drawn cup was cut out along the RD and TD as shown in Figure 3. The specific sampling positions were bottom, corner and wall region along RD, respectively.

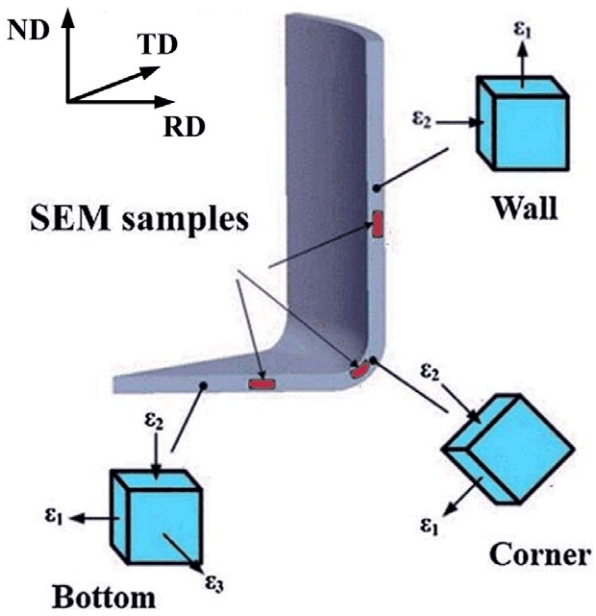


Fig. 3. Diagram of sampling from the cylindrical part

## 3. Results and discussion

### 3.1. Microstructure and mechanical property of hot-rolled and annealed composite plates

#### 3.1.1. Microstructure

Figure 4 (a) and (b) show SEM images and EDS line scan analysis of hot-rolled plates and annealed plates at Q235/410 interface, respectively. The interface layer thickness of the original hot-rolled plate is 2~4 μm. While it increases to 8-10 μm after annealing due to the further diffusion of Fe, Cr, C elements. As shown in EDS line scanning spectrum, high concentration of carbon element was present in the interface of the hot-rolled plate, which became more obvious in the annealed plate. According to Ernst et al. [20]; Matula et al. [21], the diffusion coefficients of carbon and chromium in austenite are $D_{carbon} = 1.45 \times 10^{-7}$ cm$^2$/s, and $D_{Chromium} = 3.9 \times 10^{-19}$ cm$^2$/s, respectively, Therefore, the diffusion of carbon atoms is easier than chromium. Moreover, the affinity of C and Cr is much greater than that of C and Fe. As a result, carbon atoms diffuse to 410 stainless steel side across the bonding interface and combine with chromium atoms to form chromium carbide. The chromium carbide prevents Cr diffusion to the carbon steel, leading to the increase of carbon concentration in the interface adjacent to 410 stainless steel side.

Figure 5 shows the metallographical microstructure of the original hot-rolled plate and annealed plate. Figure 5(a) shows there is a decarburized layer entirely composed of ferrite (F) with a thickness of 45-50 μm adjacent to Q235/410 interface, while F (in light) and pearlite (P) (in black) structure are present in Q235 carbon steel base away from the interface. The F grains of decarburized layer are slightly coarser than those of Q235 carbon steel. It is related to carbon diffusion during hot rolling. Upon heating to 1030°C and holding for 1 h before rolling, the redistribution of carbon element in the carbon steel occurs during the transformation from P and F into austenite (A), and the excessive carbon content may inhibit the growth

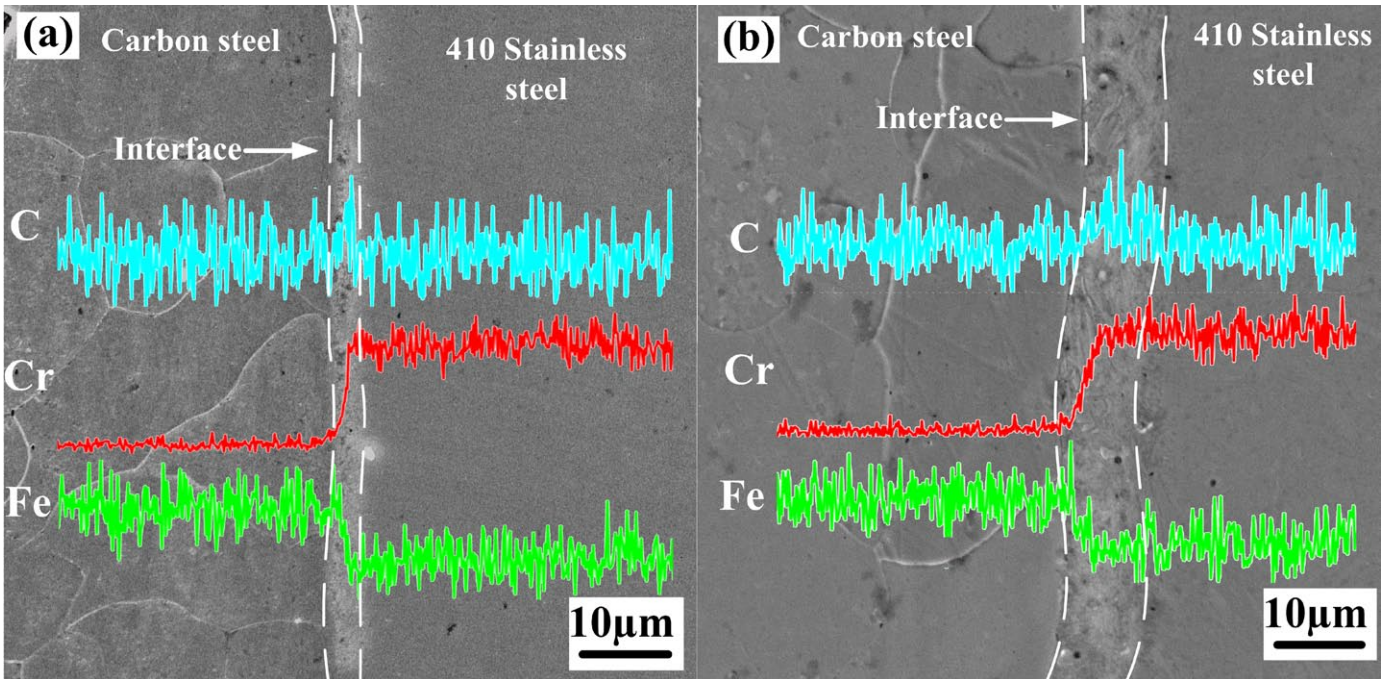


Fig. 4. Element line scanning spectrum of interdiffusion layer: (a) original hot-rolled plate and (b) annealed plate

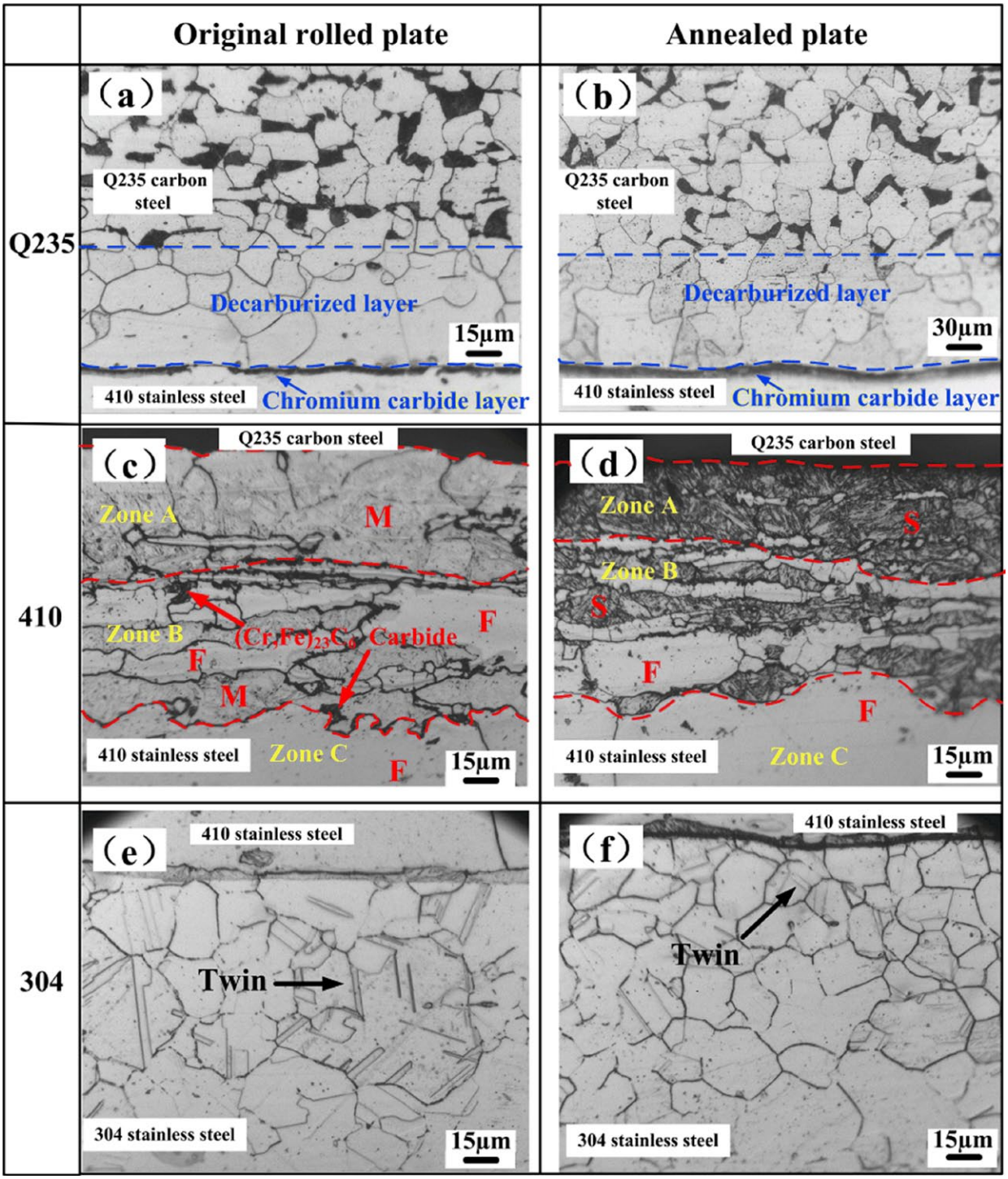


Fig. 5. OM images of different component plates in hot-rolled (a)(c)(e) and annealed states (b)(d)(f)

of A [22-23], resulting in finer A grains which are tranformed to finer proeutectoid F and eutectoid P after hot-rolling and cooling [24-25]. While near Q235/410 interface, carbon element in the carbon steel diffuses to the interface upon heating to form decarburization layer, which promotes the formation and growth rates of A grains [26] producing coarser A grains that are decomposed to coarser ferrite grains upon cooling. After annealing at 900°C for 2 h as shown in Figure 5(b), Q235 matrix microstructure becomes more uniform with carbon diffusion from P to form tiny cementite particles in F grains. And the thickness of the decarburized layer significantly increases to 80~90 μm with the further diffusion of carbon element, and the F grains both in carbon steel base and decarburized layer coarsen with the growth of A grains during annealing. Considerable black fine cementite particles are dispersedly distributed in F matrix due to quite lower solubility of carbon in F than in A upon cooling.

Figure 5(c) shows that hot-rolled 410 stainless steel interlayer consists of coarse M (Zone A), remanent M and F and Chromium carbide mixture (Zone B) and F (Zone C). Zone C is

F decarburization layer due to the intensive carbon diffusion from 410 (0.12%) to 304 stainless steel (0.036%) during heating prior to rolling, and leads to the carbon absence adjacent to 410/304 interface. Hence the A in 410 stainless steel in Zone C can only be transformed into F upon cooling. In the same way, only a part of F is formed in Zone B away from 410/304 interface with relative more carbon present. There are a lot of fine $(Cr, Fe)_{23}C_6$ carbide precipitates at the grain boundary in Zone A and B due to carbon diffusion from carbon steel and the good affinity between C and Cr elements. Pommier et al. [27-28] reported that the formation of $Cr_{23}C_6$ carbides resulted in sensitization: depletion of the local concentration of chromium element in the grain boundary. As indicated in Figure 5(d), M in Zone A and Zone B in as-rolled 410 stainless steel has transformed into much finer needle-like sorbite (S) after annealing at 900°C for 2 h which is equivalent to high temperature tempering for 410 stainless steel. And the strength and toughness of 410 stainless steel match well while maintaining a good corrosion resistance. For 304 stainless steel as shown in Figure 5(e) and Figure 5(f), A grains become finer and twins in rolled plate [29] are considerably reduced after annealing, which eliminates work hardening caused by hot rolling and greatly improves the cold deformation ability of 304 stainless steel.

### 3.1.2. Ambient-temperature tensile property

Figure 6(a) shows ambient-temperature tensile properties of the hot-rolled plates and the annealed plates. The yield strength, ultimate strength and elongation are summarized in Figure 6(b). The average ultimate strength and yield strength of the annealed composite plate along RD, 45°, TD are 459.02 MPa and 275.61 MPa, which are considerably lower than the hot-rolled plate. However, the elongation (48.21%) increases obviously. And the heterogeneity in ductility and toughness are greatly eliminated, which will be beneficial to subsequent cold deep drawing of the composite plate. Such change in tensile mechanical properties of the composite plates after annealing are closely related to the microstructure evolution of three component plates, that is, the reduction of P and increase of F grain size in Q235, the transformation from coarse M to fine needle-like S in 410 stainless steel, the A grain refinement and twins reduction in 304 stainless steel after annealing.

Figure 7 shows the macroscopic and microscopic tensile fracture morphology of the hot-rolled composite plate, which can be obviously divided into five layers. Large, deep and dense equiaxed dimples are formed in the carbon steel, indicating that the layer has good plasticity. There are three layers in illustration α. The upper layer is a ductile fracture of the decarburized layer, showing a serpentine slip ripple pattern. The interlayer (Q235/410 interface layer) is the hard brittle phase of chromium carbide and shows a brittle fracture. The lower layer is 410 stainless steel. The 410 stainless steel in the illustration β shows the plastic fracture morphology with large and deep dimples. The lower layer in the illustration β is 304 stainless steel. Because 304

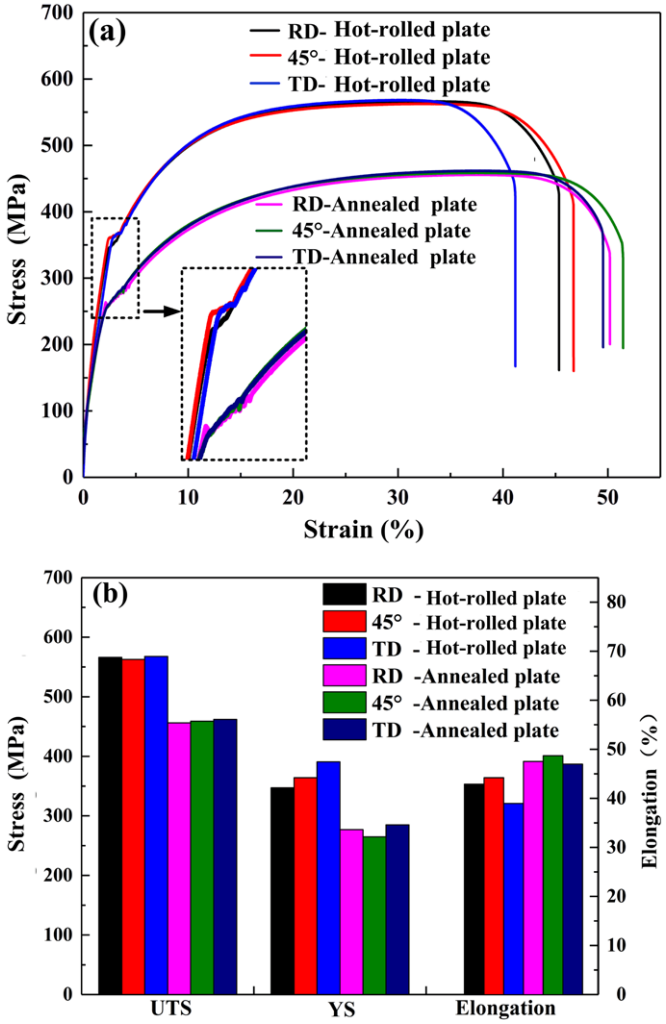


Fig. 6. Ambient-temperature tensile properties of the hot-rolled plates and the annealed plates

stainless steel is located in the shear lip position of the fracture surface, it presents a typical cutting fracture and a smooth fracture appears in this layer. There is no obvious interlaminar delamination or fracture at the interface of Q235/410 or 410/304, and no obvious dividing line is even observed at the 410/304 interface. The results show that the rolling effect of the composite plate is excellent and the quality of interlayer bonding is high.

### 3.1.3. Hardness distribution

The hardness values measured along the thickness direction of the as-rolled and annealed three-layer plates are summarized in Figure 8. The hardness of Q235 carbon steel and 304 stainless steel decrease after annealing and reach a stable value because of the grains growth in carbon steel and the elimination of twins and dislocation in 304 stainless steel. Also, the hardness of 410 stainless steel significantly diminishes because of the transformation of M into S. While the hardness both of Q235/410 and 410/304 interfaces slightly increase due to the alloying elements diffusion and the formation of hard chromium carbide at Q235/410 interface.

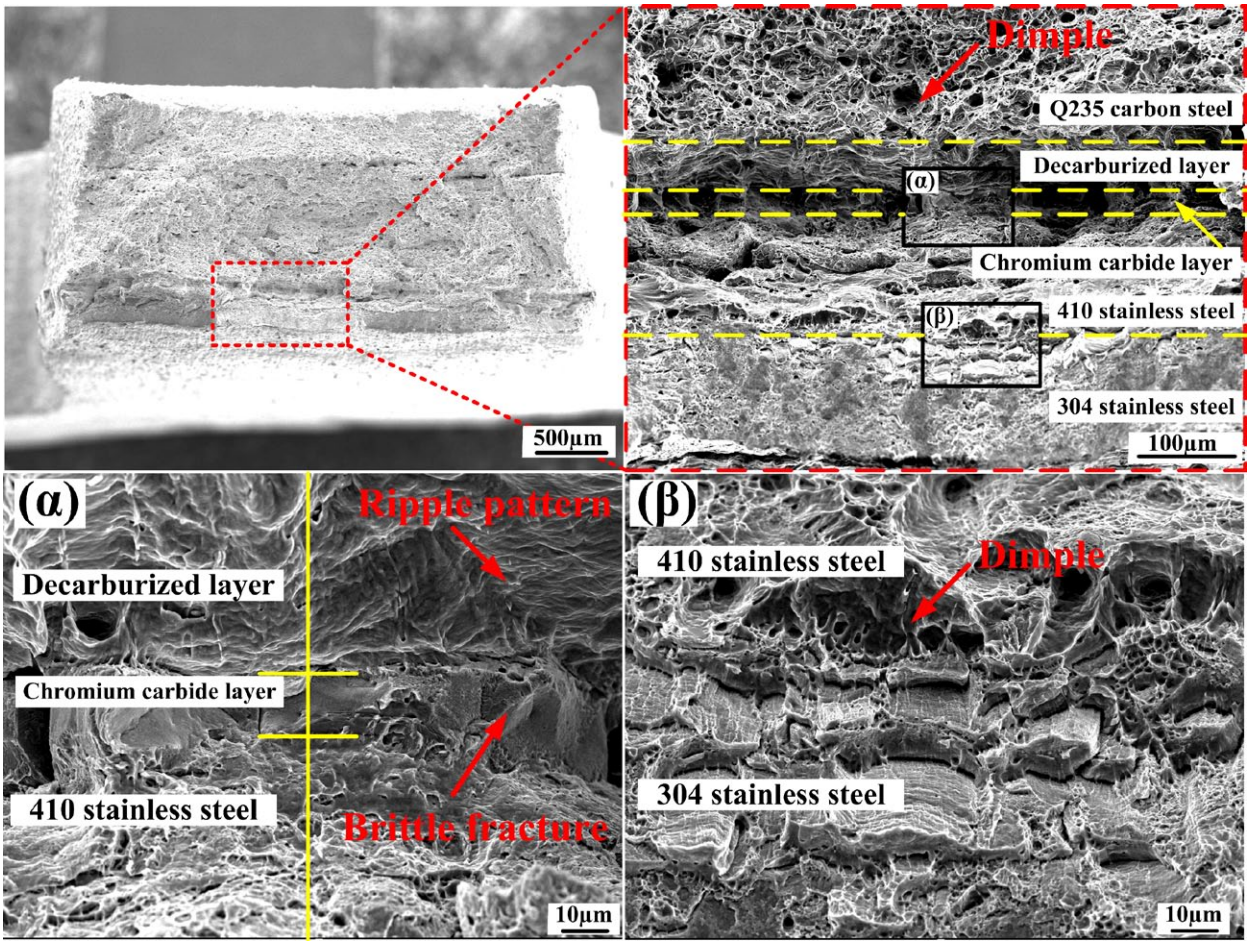


Fig. 7. The macroscopic and microscopic tensile fracture morphology of the hot-rolled composite plate

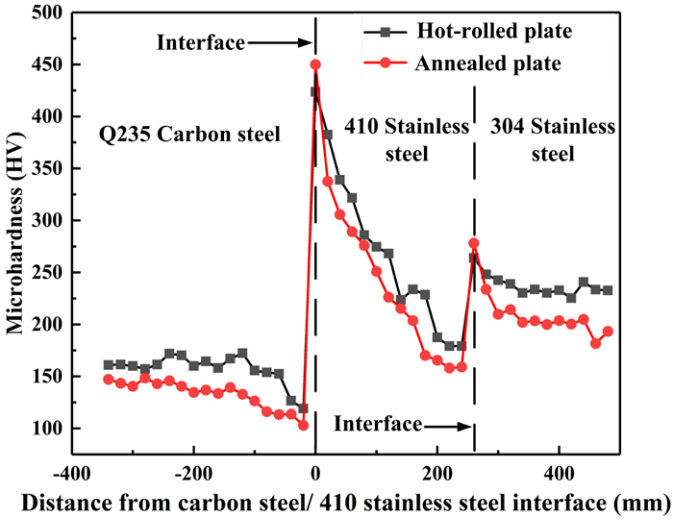


Fig. 8. Hardness distribution adjacent the Q235/410 interface

### 3.1.4. Roughness and 3D topography

Figure 9 shows the 3D topography of the both surfaces of the hot-rolled plate and annealed plate. Based on the 3D topography, roughness of these surfaces are also measured and listed in TABLE 3. The roughness of both surfaces of the annealed plate is larger than that of the hot-rolled plate and the roughness of the carbon steel surface is always larger than 304 stainless steel whether it is hot-rolled plate or annealed plate.

TABLE 3

Roughness of different surfaces

| Surface | Roughness (mm) |
|---|---|
| Carbon steel side of the hot-rolled plate | 1.428 |
| 304 stainless steel side of the hot-rolled plate | 0.927 |
| Carbon steel side of the annealed plate | 2.141 |
| 304 stainless steel side of the annealed plate | 1.596 |

## 3.2. Deep drawing behaviors of hot-rolled and annealed composite plates

### 3.2.1. LDR analysis

The samples of the four groups with a diameter 105 mm or more are selected in Figure 10. The green numbers in Fig. 10(a) represent the samples that reach LDR, while the blue represent the samples that the fracture occur for the first time in this group. The drawn cups show that the fracture of the samples always occurs in the corner region. The LDR of the groups A~D

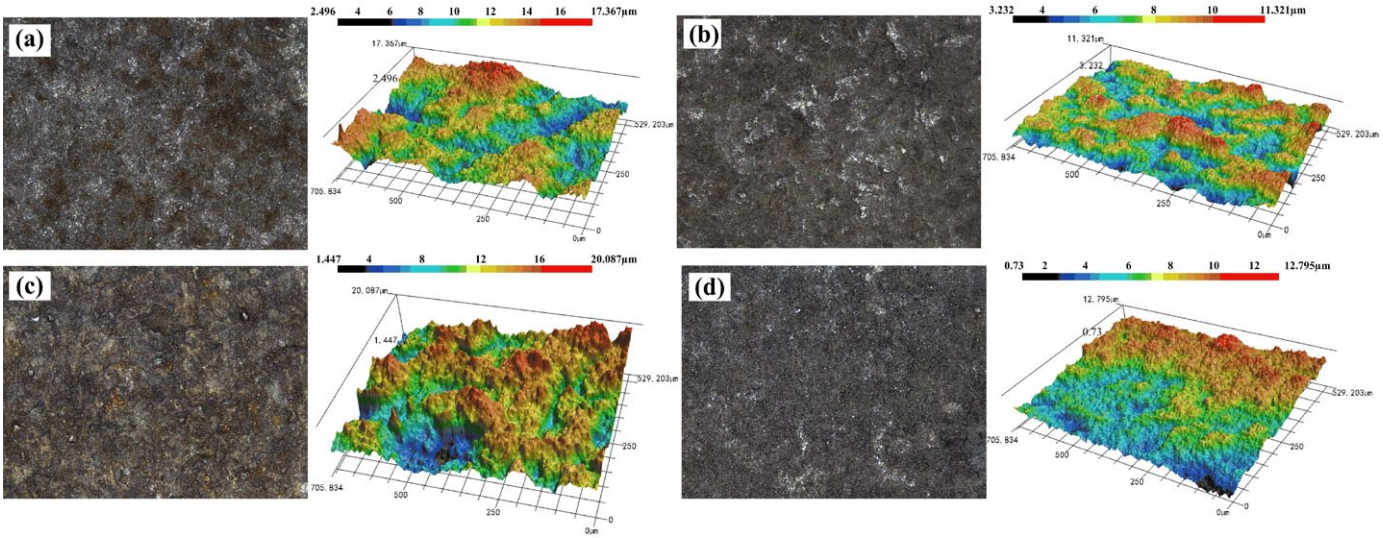


Fig. 9. 3D topography of (a) carbon steel of the hot-rolled plate, (b) 304 stainless steel of the hot-rolled plate, (c) carbon steel of the annealed plate and (d) 304 stainless steel of the annealed plate

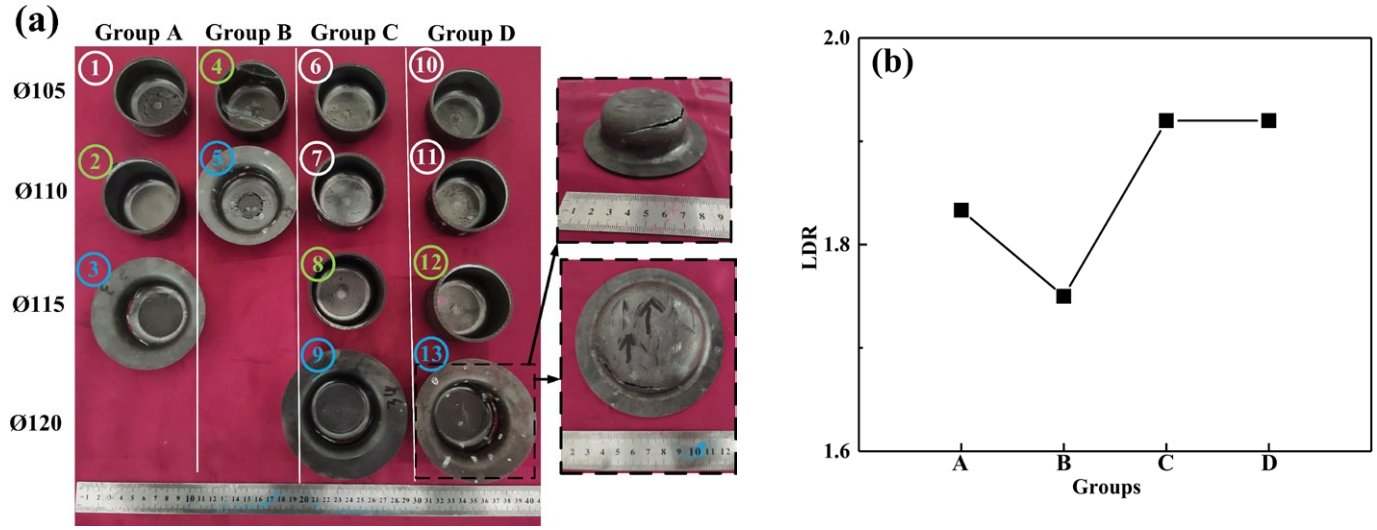


Fig. 10. Deep drawing results of the composite plates in different groups: (a) drawn cups; (b) LDR values

are 1.83, 1.75, 1.92 and 1.92, respectively. It is indicated that the drawability of hot-rolled plates greatly differs from various contact surfaces, group A with the 304 stainless steel contacting the die is better than group B with Q235 carbon steel contacting the die. While such difference no longer exists with the annealing for the hot-rolled plates, namely, whichever 304 stainless steel or Q235 carbon steel contacting the die the LDR are identical.

Figure 11 schematically represents the stress distribution of the composite plates during deep drawing. It is found that the deformation is mainly concentrated in the die fillet zone and flange zone. In group A, 304 stainless steel layer is subjected to the compressive stress applied by the punch at the die fillet, which will reduce the residual tensile stress caused by rolling (mainly in 304 stainless steel) and improve its ductility. In group B, however, it will bear the tensile stress caused by the punch while maintaining the residual tensile stress, which will greatly accelerate the crack formation and drastically diminishes the deep drawing formability. In addition, because the roughness of the carbon steel surface is greater than that of 304 stainless steel, the sample bear greater friction force at the punch fillet when carbon steel is on the inside (Group A). The friction force at the yellow circle will not change because both surfaces contact the mould. The greater friction at the punch fillet leads to greater force in the force transmission zone. Therefore, the deeper cylinder is drawn by the forming machine and better drawability of the sample is also obtained. The improved identical deep drawabilities of the annealed composite plates for various contact surfaces with the die in group C and D are attributed to the elimination of work hardening and residual stress in stainless steel and the improved ductility and toughness in component plates resulting from microstructure evolution caused by annealing. The effect of roughness difference between the two surfaces on the drawability is reduced due to the better ductility.

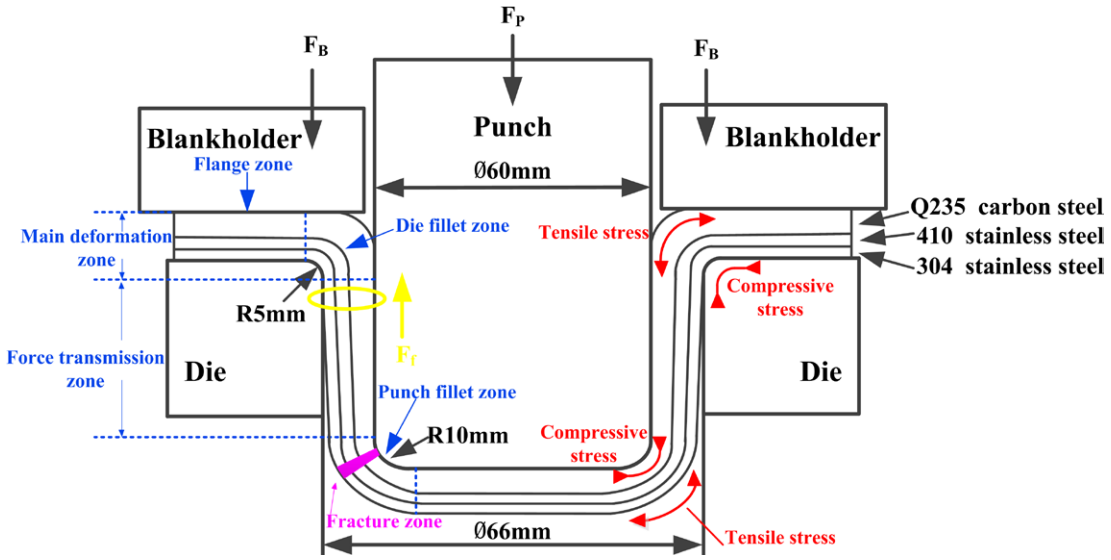


Fig. 11. Stress analysis of the composite plates during deep drawing process

### 3.2.2. Thickness strain distribution

The thickness strains are plotted at the angles of RD, 45° and TD as a function of the distance from the bottom center, as illustrated in Figure 10. It can be noted that there are two obvious thinning positions (labeled Stage 1 and Stage 2 in Fig. 12(a)) located at the corner and wall. With a punch radius of 30 mm and a punch fillet radius of 10 mm, the corner region starts at 20 mm

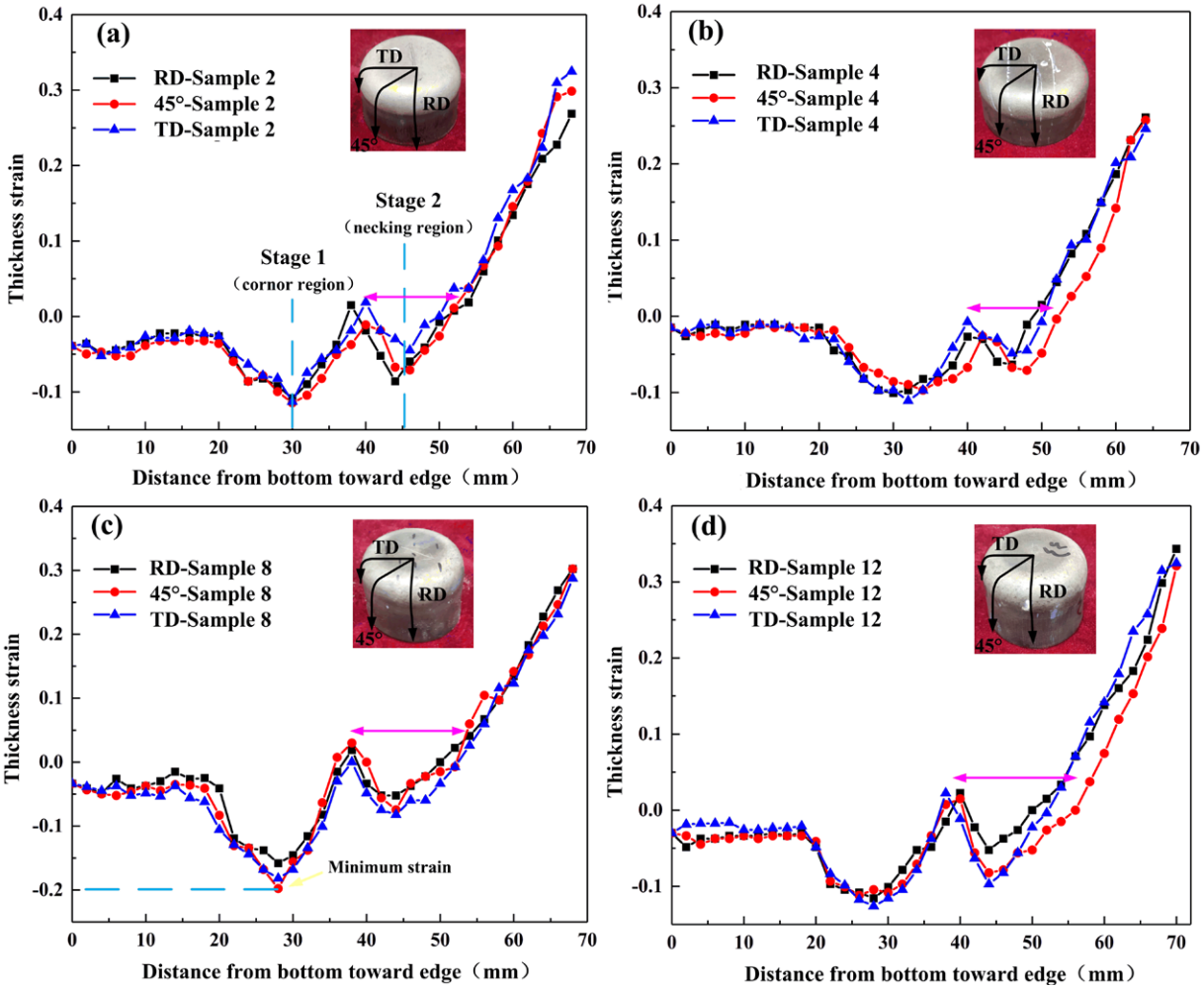


Fig. 12. Thickness strains along RD, 45° and TD of the drawn cup in different samples: (a) Sample 2, (b) Sample 4, (c) Sample 8 and (d) Sample 12

and ends at 35.7 mm (the arc length of the fillet is 15.7 mm). The thickness strain of the corner region is smaller than the necking region and the minimum thickness strain is –0.195. So the corner region is most likely to fracture and it is consistent with the facts. The necking region at 45 mm is therefore about 10 mm above the upper end of the corner, and the SEM sample of wall is cut off from here. As the punch moves, the deformation at the corner region contacting the punch-nose is restricted due to the friction, while the necking region has a small cross-sectional area to transmit drawing load, so the deformation is transferred from the corner to the necking region.

The wall region of drawn cup exhibits an increase in thickness from the necking region toward the edge region of the cup due to the continuous increasing of thickness in the flange under the tangent pressure during deep drawing [30]. The thickness strain distribution of the cup in RD, 45° and TD is basically similar owing to the isotropy of the steel sheets. It can also be noted that the average length of necking region and the minimum thickness strain of sample 2 and 4 are less than those of sample 8 and 12. This is because the annealed plate has higher ductility.

### 3.2.3. Deep drawing force

The punch load versus displacement curves are shown in Figure 13. In each group, the peak drawing force increases with the increase of the sample diameter. This is because the larger the diameter is, the more intense the metal flow required for complete forming is, which leads to the increase of forming force.

For the hot-rolled plate, the peak drawing force of sample 4 is less than that of the sample 1 with the same diameter. For the annealed plate, the peak drawing forces of sample 10, 11, 12 is less than that of sample 6, 7, 8 with the same diameter, respectively. Because the fracture mainly occurs at the corner (purple zone in Figure 9), the deformation resistance here directly affects the peak force. The outer sheet bears greater tensile stress at the corner and the deformation resistance of carbon steel is lower than that of stainless steel in both composite plates. In addition, the large roughness of the carbon steel leads to great friction at the corner, which causes the fracture of the sample with carbon steel on the inside of the cylinder (sample 1 and sample 6, 7, 8) to occur under greater drawing force. As a consequence of the drop in the ultimate strength caused by annealing, the peak forces

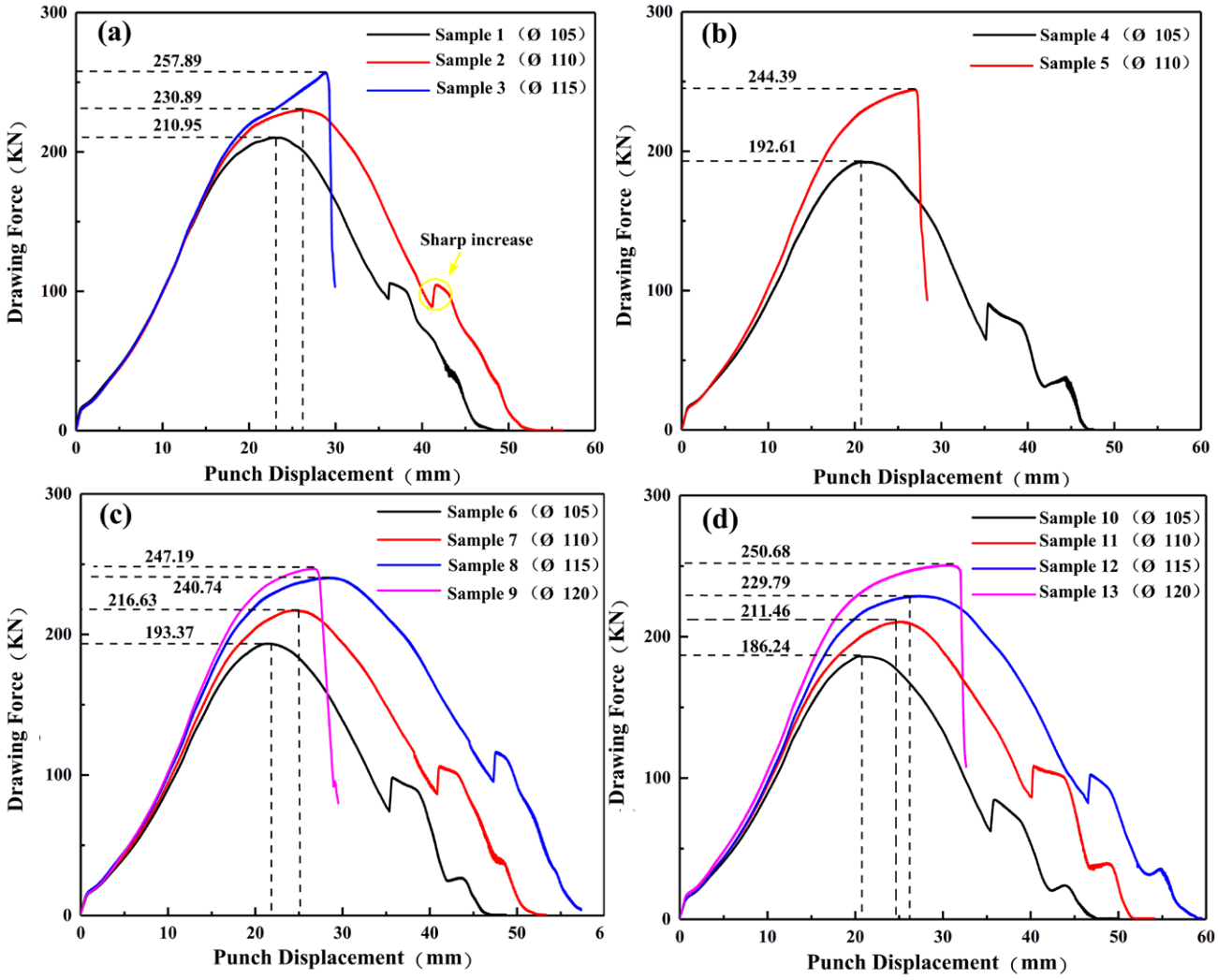


Fig. 13. Punch force versus displacement of Q235 carbon steel/410/304 stainless steel composite plates drawn cup in different groups: (a) group A, (b) group B, (c) group C and (d) group D

of sample 1, 2 and sample 4 are larger than that of sample 6, 7 and sample 10. It can also be noted that there is one or two sharp increase in each curve except the fracture one. This is due to the thickness increase after necking region, which increases the friction between the plate and die.

### 3.2.4. Interface structure of deep-drawn plates

The strain states and cross-sectional SEM images of the cylinders drawn by hot-rolled annealed plates at the bottom, corner and wall region are shown in Figure 14 and Figure 15. The $\varepsilon_1$, $\varepsilon_2$, $\varepsilon_3$ represent the radial, thickness and tangential strain, respectively.

Figure 14(a)-(c) exhibit the interface microstructure evolution of sample 2. The microstructure of the interface at the bottom region are similar to the undrawn plate and only small crack is observed (Fig. 14(c)). Because bottom region has experienced almost negligible deformation (with thickness strain of –0.05~0). It is shown in Figure 14(b) that there are more cracks at the corner region than those at other regions. Because there is a severe thinning where the fracture occurs most easily. It is worth to notice that the transverse crack (perpendicular to the interface) taking place within the brittle chromium carbide propagates to 410 stainless steel. Because the microhardness of the 410 stainless steel is higher than that of the decarburized layer in carbon steel and the chromium carbide is the hardest (Fig. 8), indicating that the 410 stainless steel lacks of accommodation to the plastic deformation compared with Q235 carbon steel. In addition, the 410 stainless steel of sample 2 subjected to greater tensile stress is on the outside of the cylinder where cracks occur more easily.

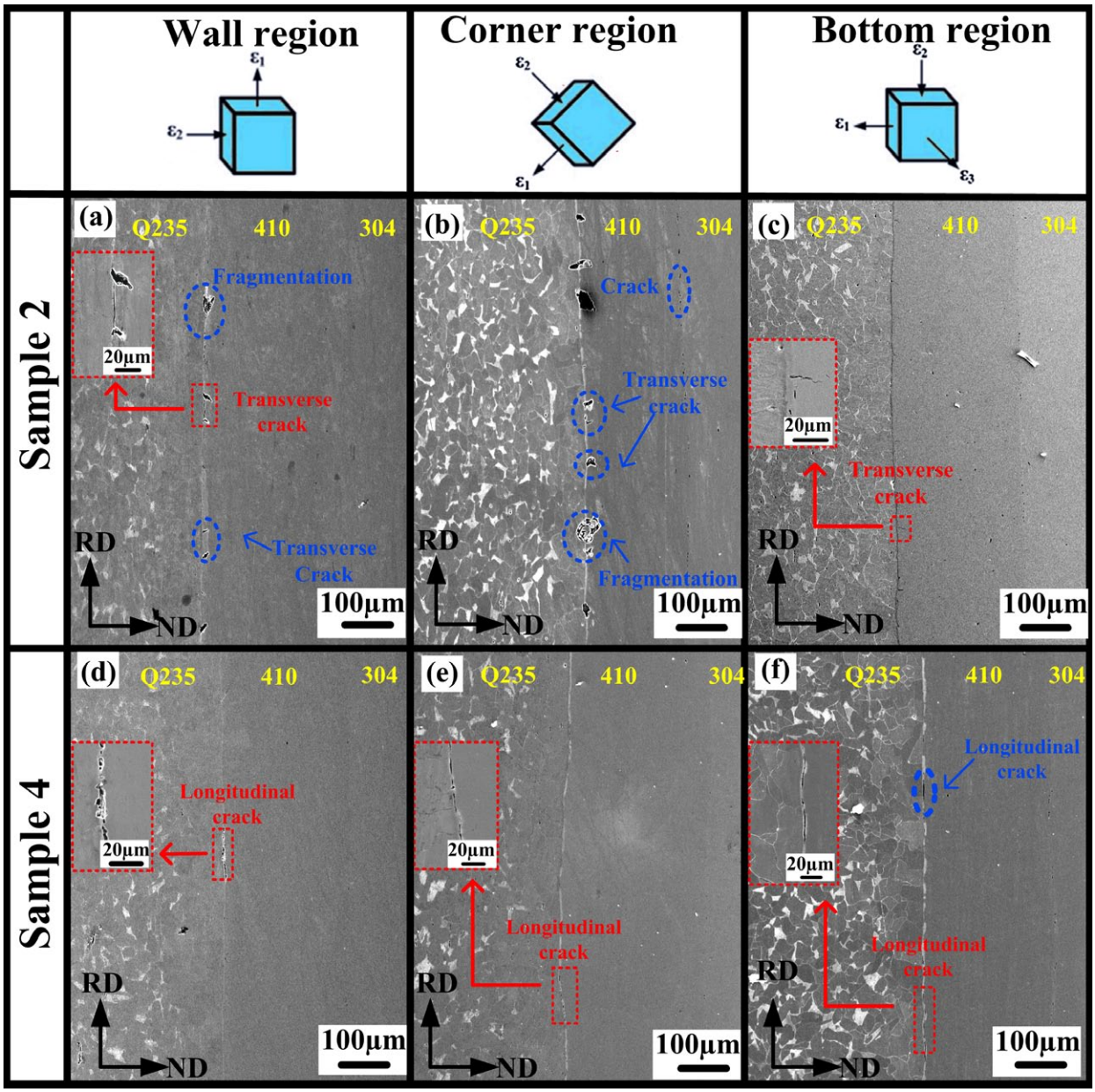


Fig. 14. Microstructure evolution of the Q235/410 interface of the cylinder drawn by the hot-rolled plates: (a) wall, (b) corner, (c) bottom of the sample 2; (d) wall, (e) corner, (f) bottom region of the sample 4

Figure 14(d)-(f) exhibit the interface microstructure evolution of sample 4. More small longitudinal cracks (parallel to the interface) were observed at three different regions compared with sample 2. After the crack is initiated at the brittle chromium carbide, the crack cannot extend to the softer carbon steel subjected to a greater tensile stress. Hence, longitudinal crack is more likely to be formed. For the 410/304 interface, almost no cracks occur except for the corner of sample 2. This may be because the difference between the two stainless steel is smaller and the bonding is stronger.

Figure 15 exhibits the Q235/410 interface microstructure evolution of sample 8 and 12. Like the cylinder drawn by the hot-rolled plate, there are almost no cracks at the bottom region. More transverse cracks are observed in sample 8 and more longitudinal cracks are observed in sample 12. It is clear that there are much fewer cracks than the hot-rolled plate, which is related to the interfacial bonding strength. The chromium carbide phase shows strong hardening and high deformation coordination after annealing. Therefore, the propagation of crack could be suppressed by annealing and the cylinder has a more favorable drawability.

## 4. Conclusions

Deep drawing behaviors of hot-rolled Q235 carbon steel/410/304 stainless steel composite plate in terms of various contacting surface with the die and annealing were investigated at the room temperature. The main conclusions are as follows:

(1) Contacting side of the hot-rolled Q235 carbon steel/410/304 stainless steel composite plate with the die has a great effect on its deep drawability. The LDR of the composite plate

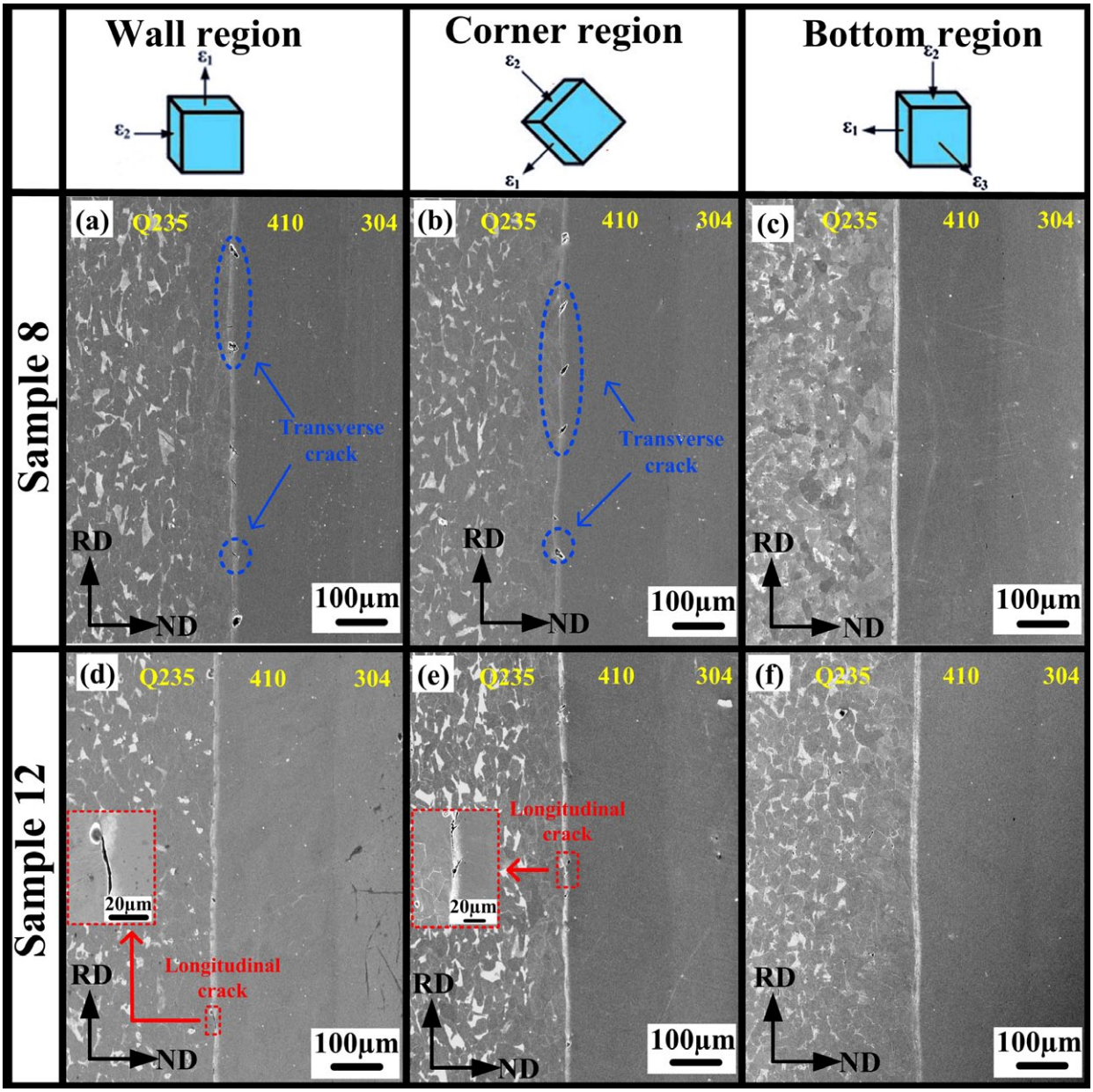


Fig. 15. Microstructure evolution of the Q235/410 interface of the cylinder drawn by the annealed plates: (a) wall, (b) corner, (c) bottom region of the sample 8; (d) wall, (e) corner, (f) bottom region of the sample 12

with O235 carbon steel contacting the die is 1.75, while 1.83 with 304 stainless steel contacting the die due to the different mechanical responses to the tensile stress at the die fillet and different roughness of the two surfaces. And it is 1.92 whichever side contacts the die due to the enhancement of plasticity and stress relief after annealing.

(2) Two obvious thinning positions (corner region and necking region) located at the corner and wall of the cylinder were observed. The thickness strain of the corner region is smaller than the necking region and the minimum thickness strain is -0.195. The average length of necking region and the minimum thickness strain of the cylinders drawn by hot-rolled plates are less than those drawn by annealed plates due to higher ductility of the annealed plate.

(3) Because the outer sheet of the composite plate is subjected to the tensile stress at the corner region where the fracture mainly occurs and the deformation resistance of carbon steel is always lower than stainless steel, whether the sample is annealed or not, the peak drawing force of the sample with carbon steel contacting die is always less than that with carbon steel contacting punch under the same diameter. In addition, the large roughness of the carbon steel leads to great friction at the corner, which causes the fracture of the sample with carbon steel contacting die to occur under greater drawing force.

(4) The cylinders with the stainless steel contacting the die show more transverse cracks than that with the opposite contact surface. Because the stainless steel is subjected to a large tensile stress on the outside, and the hardness of the 410 stainless steel is higher than carbon steel. Moreover, the composite plates show better drawability after annealing with less cracks appeared because of the stronger bonding strength and higher deformation coordination of the chromium carbide phase.

**Acknowledgements**

This work was supported by the National Key R & D program: high-quality metal composite plate efficient preparation principle and technical basis (2018YFA0707300), the Major Program of National Natural Science Foundation of China (U1710254), Youth Science Foundation Project of National Natural Science Foundation of China (51905372) and General Program of National Natural Science Foundation of China (51975398, 51974196).

## REFERENCES

[1] Q.X. Huang, X.R. Yang, L.F. Ma, C.L. Zhou, G.M. Liu, H.B. Li, J. Iron Steel Res. Int. **21** (10), 931-937(2014).

[2] S.C. Pan, M.N. Huang, G.Y. Tzou, S.W. Syu, J. Mater. Process. Technol. **177** (1-3), 114-120 (2006).

[3] Y. Jing, Y. Qin, X. Zang, Y. Li, J. Mater. Process. Technol. **214** (8), 1686-1695 (2014).

[4] S. Zhang, H. Xiao, H. Xie, L. Gu, J. Mater. Process. Technol. **214** (6), 1205-1210 (2014).

[5] L. Li, K. Nagai, F. Yin, Sci. Technol. Adv. Mater. **9** (2), 23001 (2008).

[6] B.X. Liu, S. Wang, W. Fang, F.X. Yin, C.X. Chen, Mater. Charact. **148**, 17-25 (2019).

[7] C.X. Chen, M.Y. Liu, B.X. Liu, F.X. Yin, Y.C. Dong, X. Zhang, F.Y. Zhang, Y.G. Zhang, Fusion Eng. Des. **125**, 431-441 (2017).

[8] B.X. Liu, S. Wang, W. Fang, J.L. Ma, F.X. Yin, J.N. He, J.H. Feng, C.X. Chen, Mater. Chem. Phys. **216**, 460-467 (2018).

[9] B.X. Liu, F.X. Yin, X.L. Dai, J.N. He, W. Fang, C.X. Chen, Y.C. Dong, Mater. Sci. Eng. A. **679**, 172-182 (2017).

[10] B.X.Liu, S. Wang, C.X. Chen, W. Fang, J.H. Feng, X. Zhang, F.X. Yin, Appl. Surf. Sci. **463**, 121-131 (2019).

[11] Z. Dhib, N. Guermazi, M. Gaspérini, N. Haddar, Mater. Sci. Eng. A. **656**, 130-141 (2016).

[12] Y. Chino, X. Huang, K. Suzuki, K. Sassa, M. Mabuchi, Mater. Sci. Eng. A. **528** (2), 566-572 (2010).

[13] J. Singh, M.S. Kim, S.E. Lee, E.Y. Kim, J.H. Kang, J.H. Park, J.J. Kim, S.H. Choi, Mater. Sci. Eng. A. **729**, 370-384 (2018).

[14] M.X. Guo, J. Zhu, Y. Zhang, G.J. Li, T. Lin, J.S. Zhang, L.Z. Zhuang, Mater. Charact. **132**, 248-259 (2017).

[15] D. Ghaffari Tari, M.J. Worswick, S. Winkler, J. Mater. Process. Technol. **213** (8), 1337-1347 (2013).

[16] F.K. Chen, K.H. Chiu, J. Mater. Process. Technol. **170** (1), 181-186 (2005).

[17] M. Torkar, F. Tehovnik, B. Podgornik, Eng. Fail. Anal. **40**, 1-7 (2014).

[18] R. Padmanabhan, M.C. Oliveira, J.L. Alves, L.F. Menezes, Finite Elem. Anal. Des. **43** (14), 1062-1067 (2007).

[19] J. Lade, B.N. Banoth, A.K. Gupta, S.K. Singh, J. Iron Steel Res. Int. **21** (12), 1147-1151 (2014).

[20] F. Ernst, Y. Cao, G.M. Michal, A.H. Heuer, Acta Mater. **55** (6), 1895-1906 (2007).

[21] M. Matula, L. Hyspecka, M. Svoboda, V. Vodarek, C. Dagbert, J. Galland, Z. Stonawska, L. Tuma, Mater. Charact. **46** (2), 203-210 (2001).

[22] J. Park, J.S. Kim, M. Kang, S.S. Sohn, W.T. Cho, H.S. Kim, S. Lee, Sci. Rep. **7**, 40231 (2017).

[23] M. Jung, W. Cho, J. Park, J.G. Jung, Y.K. Lee, Mater. Charact. **94**, 161-169 (2014).

[24] N.V. Rao, D.S. Sarma, S. Nagarjuna, G.M. Reddy, Met. Sci. J. **25** (11), 1387-1396 (2009).

[25] B. Hwang, H.S. Lee, Y.G. Kim, S. Lee, Mater. Sci. Eng. A. **402** (1), 177-187 (2005).

[26] Y. Sidor, F. Kovac, T. Kvackaj, Acta Mater. **55** (5), 1711-1722 (2007).

[27] H. Pommier, E.P. Busso, T.F. Morgeneyer, A. Pineau, Acta Mater. **103**, 893-908 (2016).

[28] K.J. Kim, J. Ginsztler, S.W. Nam, Mater. Lett. **59** (11), 1439-1443 (2005).

[29] Y.F. Shen, X.X. Li, X. Sun, Y.D. Wang, L. Zuo, Mater. Sci. Eng. A. **552**, 514-522 (2012).

[30] H. Zhang, G. Huang, J. Fan, H. Jørgen Roven, F. Pan, B. Xu, Mater. Sci. Eng. A. **608**, 234-241 (2014).